

Comparative study of ESR spectra in incommensurate antiferromagnets

S. S. Sosin¹, L. A. Prozorova, M. E. Zhitomirsky*

P. L. Kapitza Institute for Physical Problems RAS, 117334 Moscow, Russia

**Commissariat à l'Energie Atomique, DMS/DRFMC/SPSMS, 38054 Grenoble, France*

Submitted 9 December 2003

The electron spin resonance is studied for noncollinear low-dimensional antiferromagnets RbMnBr₃ and RbFe(MoO₄)₂ in a wide range of frequencies and fields. Both compounds have incommensurate spin structures appearing due to a low-symmetry distortion of an ideal hexagonal crystal lattice. Magnetic field applied in the spin plane induces a first order transition into the commensurate phase. The low-energy resonance branch corresponding to a uniform oscillation of the spin system in the easy-plane is observed in the two compounds both in incommensurate and commensurate phases, with a dramatic change of the spectra taking place near the transition field. The resonance spectrum of a nearly commensurate spin structure with long-wave modulations is analyzed in clean and dirty limits in the framework of a hydrodynamic approach. The resonance branch with steep field dependence in the incommensurate state is attributed to the acoustic mode with the gap resulted from pinning of local domain walls (discommensurations) on defects of the crystal structure.

PACS: 75.50.-y, 76.50.+g

1. Introduction. Helical spin structures with incommensurate long wave-length modulations is an interesting type of magnetic ordering [1]. They appear, generally, for two reasons: (i) when the symmetry of the crystal structure allows the Lifshitz invariant (of exchange or relativistic origin) or (ii) in the case of an 'accidental' instability of a commensurate state due to competing exchange interactions. The compound RbMnBr₃ studied in this work belongs to the systems of the first type while the origin of the low temperature incommensurate state in RbFe(MoO₄)₂ is still under debate.

The two materials crystallize into hexagonal structure belonging to the same class of the point symmetry $\bar{3}m1$ (D_{3d}), space group $P6_3/mmc$ (D_{6h}^4) for RbMnBr₃ [2] (as for other ABX₃ systems) and $P\bar{3}m1$ (D_{3d}^3) for RbFe(MoO₄)₂ which undergoes phase transitions into different low-symmetry states on cooling. The crystal structure of RbMnBr₃ below $T_c = 220$ K is characterized by weak orthorhombic distortions with zigzags of magnetic ions shifted alternately up and down from the basal plane (space group $Pbca$) [3]. An incommensurate helical structure with magnetic Bragg peaks at $\mathbf{Q} = (h/8 + \xi, h/8 + \xi, l)$, where h and l are integers and $\xi = 0.0183 \pm 0.0004$, has been observed in the neutron scattering experiment below $T_N = 8.5$ K in zero magnetic field [4]. Microscopically, it can be described in terms of the row model assuming exchange interaction

along zigzags to be somewhat different from those in other two in-plane directions [5, 6]. The initial high symmetry structure of RbFe(MoO₄)₂ also reveals distortions below $T_c = 180$ K [7], but the space group for this structure is not exactly determined. The ordered magnetic phase forming at $T_N = 3.8$ K appears to be incommensurate helix with the wave vector $\mathbf{Q} = (1/3, 1/3, 0.41)$ [8]. Presumably, it results from inequality of the transversal exchange bonds between magnetic ions in neighboring planes.

Both structures have a strong easy-plane anisotropy keeping all spins inside the basal plane. Magnetic field applied in this plane gradually makes the incommensurate structure unfavorable and produces the first order transition into the commensurate phase at $H_c \simeq 29$ kOe for RbMnBr₃ and 39 kOe for RbFe(MoO₄)₂. The resonance spectra of these multi-sublattice systems consist of several branches. Their distinct feature is a behavior of a low-energy acoustic branch which corresponds to uniform oscillations of the spin system in the easy-plane. For triangular antiferromagnets it has a dependence $\nu \propto H^3$ valid until the exchange structure is weakly distorted by magnetic field. This branch has been observed in RbMnBr₃ only in the commensurate phase and disappeared below H_c [9]. Such an end point in $\nu(H)$ was explained by an appearance of the Goldstone mode related to spontaneous translational symmetry breaking in the incommensurate phase [10]. Similar resonance branch was found in RbFe(MoO₄)₂ [11]. A fi-

¹)e-mail: sosin@kapitza.ras.ru

nite frequency resonance mode can, however, be excited at the wave vector of incommensurate modulations. We have performed a search for such a low-energy mode starting from the frequency of 3 GHz. A new resonance branch has been found in the incommensurate phase with a very steep increase towards the transition field H_c . We also present theoretical calculations for the resonance in the incommensurate phase and discuss their relation to the observed branch.

2. Experiment. Bridgman method was used to grow single crystals of RbMnBr_3 . The samples of $10 \div 100 \text{ mm}^3$ in size were cut along binary planes (perpendicular to the basal plane of the crystal) so that one could easily orient them with respect to the magnetic field. The crystals of $\text{RbFe}(\text{MoO}_4)_2$ were grown from the flux. The resulting thin plates of $1 \div 2 \text{ mm}^3$ had planes perpendicular to the C_3 -axis.

We performed a series of electron spin resonance (ESR) measurements on single crystals of both compounds in a frequency range from 3.5 GHz to 50 GHz. Three transmission-type spectrometers with various types of resonators (toroidal, rectangular and cylinder) were used in the experiment. Magnetic field up to 6 T was created by a cryomagnet. All experiments were carried out in a well ordered antiferromagnetic phase at temperatures 1.2–2.5 K significantly below corresponding Néel temperatures.

The typical absorption lines in RbMnBr_3 for the magnetic field applied in the basal plane are shown in fig.1. The records were taken in both directions of the

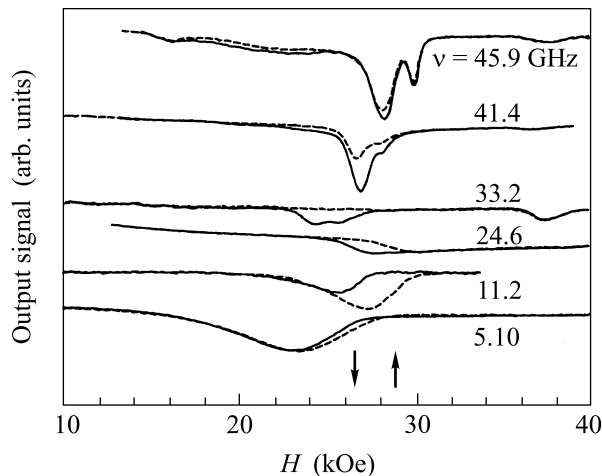


Fig.1. Field dependence of the resonance absorption in RbMnBr_3 ($T = 1.3 \text{ K}$); dashed lines - forward field sweep, solid lines - backward sweep; \uparrow and \downarrow mark the transitions for the forward and the backward scans respectively

field sweep. At the lowest resonance line $\nu = 5.10 \text{ GHz}$ (the low curve) the absorption appears to be almost

without hysteresis as the main part of the resonance line is far from the transition. On increasing the frequency we approach to the critical field and the hysteresis becomes more pronounced. The resonance exists below the transition and then sharply disappears at $H > 29 \text{ kOe}$. In the opposite direction it restores only at $H < 26.5 \text{ kOe}$ indicating the return to the incommensurate phase. These fields are marked by arrows in fig.1. Obviously it means that the signal observed in the frequency range 5–20 GHz corresponds to the low field phase. Subsequently, this resonance absorption is replaced by singularities in the transmitted signal at the critical fields ($\nu = 24.6 \text{ GHz}$). The resonant signal restores at higher frequencies with the inverse hysteresis. For example, at the frequency $\nu = 33.2 \text{ GHz}$ no signal is observed for a forward field sweep while a resonance absorption reveals itself on the backward scan. Further increase in frequency allows one to detect signal in both direction, with the hysteresis vanishing completely above $\nu = 46 \text{ GHz}$. In contrast to the low frequency signal, this resonance may obviously be attributed to the high field (commensurate) phase. This effect was first described in work [9] and was interpreted as an absence of an acoustic resonance mode until the transition into a commensurate spin structure [10].

The main difference with the previous results is that this branch at $H > H_c$ is split into two lines. The splitting results from orthorhombic distortions of the crystal structure removing degeneracy of the high symmetry hexagonal plane. Obviously, there should be three equivalent directions $\mathbf{x}_{1,2,3}$ (domains) of such distortions at an angle of 120° to each other. This weak anisotropy contributes to the potential energy of the spin system, thus originating the dependence of the AFMR frequency on the angles between \mathbf{x}_i and the magnetic field. We have studied this effect in more details by measuring the dependence of the resonance line in the large sample (containing all domains in roughly equal parts) on the direction of the magnetic field in the easy plane. The sample was initially oriented by one of the basal planes perpendicular to the field. In this orientation one of the domains lies in the rational direction while the other two are deviated by $\pm 60^\circ$. For this reason two lines are observed with the relative intensity 1 : 2. Rotating the sample in the easy plane one obtains the full picture including all three lines as shown in fig.2. Their angular dependencies are shifted by $\pm 60^\circ$ to each other as expected from the domain structure of the sample. The fits in the inset of fig.2 are harmonic functions with amplitudes determined by the value of the in-plane anisotropy.

Note, that the resonance lines observed at low frequencies (5.10 GHz) demonstrate a strong temperature

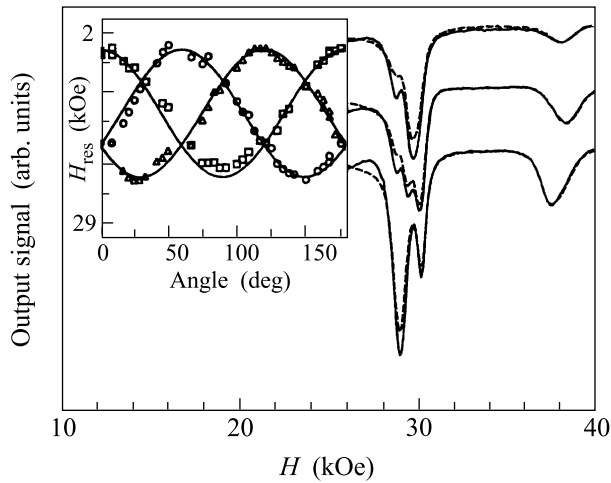


Fig.2. Resonance absorption at $\nu = 44.7$ GHz for three orientations of the crystal in the magnetic field ($T = 1.3$ K). Inset shows the angle dependence of the resonance field for each of three domains; solid lines are sinusoidal fits (see text)

dependence most likely associated with the hyperfine interaction inside Mn^{2+} ions. The hyperfine interaction leads to hybridization of nuclear and electron spin resonance modes and to appearance of the gap in the mixed spectrum $\nu^2 = \nu_e^2 + A/T$ (ν_e is the initial resonance frequency; for similar compounds CsMnBr_3 and CsMnI_3 $A \sim 50 \text{ GHz}^2 \cdot \text{K}$ [12, 13]). On increasing temperature by 0.5 K the maximum of the absorption slides from 25 kOe to 18 kOe after which the line strongly broadens

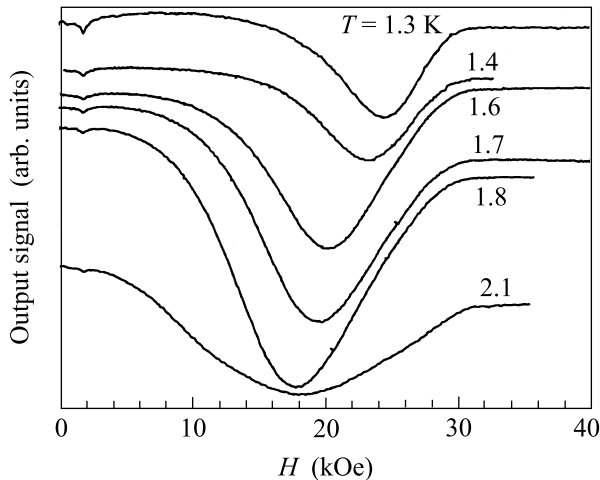


Fig.3. Temperature dependence of the resonance absorption (forward field sweep) in RbMnBr_3 at $\nu = 5.10$ GHz

and disappears (see fig.3). The resonance at 3.47 GHz and 7.11 GHz demonstrates qualitatively the same be-

havior while at other frequencies it becomes almost temperature independent in this range.

The low-frequency part of the resonance spectrum of $\text{RbFe}(\text{MoO}_4)_2$ was studied at $T = 1.3$ K (well below $T_N = 3.8$ K). The results obtained in the same frequency range as for RbMnBr_3 are represented in fig.4. The mag-

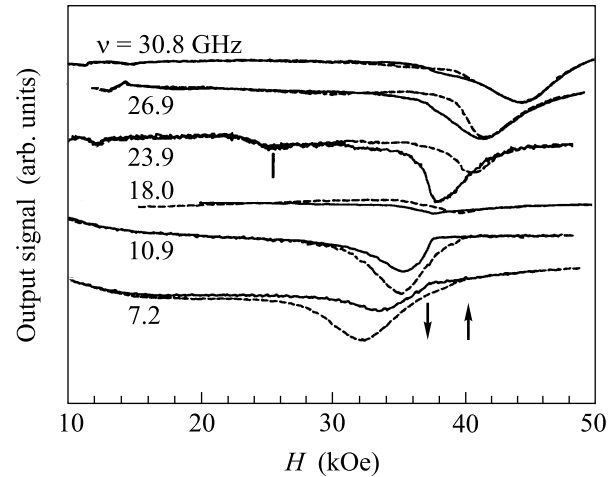


Fig.4. Field dependence of the resonance absorption in $\text{RbFe}(\text{MoO}_4)_2$ at $T = 1.3$ K; dashed lines – forward field sweep, solid lines – backward sweep; \uparrow and \downarrow mark the transitions for the forward and the backward scans respectively

netic field was applied perpendicular to the C_3 -axis. The spectrum in this frequency range consists of one low-energy relativistic and one high-energy exchange branch corresponding to the in-phase (as in RbMnBr_3) and out-of-phase oscillations of the spin planes, respectively. The intensity of the latter mode was very weak (one of the corresponding peaks is shown in fig.4 by the stroke, the other points are invisible in this scale).

The evolution of the acoustic resonance line on increasing the frequency is very similar to what has been observed in RbMnBr_3 . Namely, there is a hysteresis in the absorption depending on the position of the resonance field at a given scan. At lower frequencies the absorption corresponds to the low field phase and vice versa. In the intermediate range the signal is replaced by nonresonance singularities at the transition fields 39.5 and 37.5 kOe for a forward and backward scans respectively (indicated by up and down arrows on fig.4). For the details of the high frequency part of the spectrum see work [11].

3. Theory. An incommensurate spin structure in a magnetic system with the Lifshitz invariant can be described by long-wave length modulations of a commensurate state corresponding to a certain wave-vector \mathbf{k}_0 . In the case, when a commensurate structure is non-

collinear, a pair of orthogonal vectors \mathbf{l}_1 and \mathbf{l}_2 has to be used to describe both commensurate and incommensurate states:

$$\mathbf{S} \sim \mathbf{l}_1 \cos \mathbf{k}_0 \mathbf{r} + \mathbf{l}_2 \sin \mathbf{k}_0 \mathbf{r}. \quad (1)$$

The commensurate wave-vector $\mathbf{k}_0 = (4\pi/3a, 0, \pi/c)$ appropriate for both compounds corresponds to a triangular 120° spin structure in the basal plane with antiferromagnetically correlated layers giving six sublattices in total. Strong easy-plane anisotropy confines spins to the basal plane, hence slow rotations of $\mathbf{l}_1, \mathbf{l}_2$ can be parameterized by an in-plane angle φ . In RbMnBr_3 such modulations propagate along the a -axis: $\varphi(x)$, while for $\text{RbFe}(\text{MoO}_4)_2$ modulations are along the c -axis: $\varphi(z)$. In the following we denote the propagation direction of incommensurate modulations as x and write the corresponding hydrodynamic energy functional with the Lifshitz term in a general form [14], which is applicable to many other incommensurate systems:

$$E = \int dx \left[\frac{M}{2} (\partial_t \varphi)^2 + \frac{B}{2} (\partial_x \varphi)^2 - b (\partial_x \varphi) + A \cos n\varphi \right]. \quad (2)$$

Six sublattice antiferromagnets have a field induced anisotropy with $n = 6$ and $A \sim H^6$, while a weakly incommensurate two-sublattice antiferromagnet would have $n = 2$ and $A \sim H^2$. For vanishing anisotropy, the Lifshitz term stabilizes an incommensurate sinusoidal modulations with $\varphi = bx/B$. Sufficiently strong anisotropy stabilizes commensurate domains with $\varphi = (\pi/n)(2m + 1)$. The transition into commensurate state takes place when the energy of a single domain wall (also called soliton, kink, or discommensuration) of a width d

$$\varphi_s(x) = -\frac{\pi}{n} + \frac{4}{n} \arctan e^{x/d}, \quad d = \frac{1}{n} \sqrt{\frac{B}{A}}, \quad (3)$$

becomes positive. Such a lock-in transition occurs at the critical anisotropy

$$A_c = \frac{\pi^2 b^2}{16B}. \quad (4)$$

Below the lock-in transition a static long wave-length modulation of the \mathbf{k}_0 -structure satisfies

$$\frac{B}{2A} (\partial_x \varphi)^2 = \frac{2}{\kappa^2} - 1 + \cos n\varphi \quad (5)$$

and has a form of a soliton lattice $\varphi_0(x) = (2/n) \text{am}(x/d\kappa)$, where $\text{am}(z)$ is the elliptic amplitude and κ is the modulus of the elliptic functions. The distance between solitons is $l = 2d\kappa K(\kappa)$, where $K(\kappa) (E(\kappa))$ denote the complete elliptic integrals of the first

(second) kind. Minimization of the energy of the soliton lattice yields

$$\frac{E(\kappa)}{\kappa} = \sqrt{\frac{A_c}{A}}, \quad (6)$$

which implicitly determines the field dependence of κ . For small anisotropy $A \ll A_c$, the soliton lattice transforms into a sinusoidal modulation with a period $L = nl = (2\pi B/b)(1 + A^2 B^2/2b^4)$, whereas near A_c the intersoliton distance grows logarithmically $l = d \ln[8A_c/(A_c - A)]$.

The dynamics of the model Eq. (2) has been studied in many applications, *e.g.*, for Josephson junctions [15] and for charge-density waves [16, 17]. The excitation spectrum is obtained in the linear approximation with respect to small oscillations $\varphi(x, t) = \varphi_0(x) + \psi(x, t)$. With $\psi(x, t) \sim e^{-i\Omega t}$ the equation of motion is reduced to the Lamé equation

$$\frac{d^2 \psi}{dz^2} + \kappa^2 \left[1 + \frac{\Omega^2}{\omega_c^2} - 2 \text{sn}^2(z) \right] \psi(z) = 0, \quad (7)$$

where $z = x/d\kappa$, $\omega_c^2 = n^2 A/M$ is the resonance ($q = 0$) frequency in the commensurate state for vanishing incommensuration $b = 0$ and $\text{sn}(z)$ is the elliptic sine. The general solution of the Lamé equation is given by [18]

$$\psi(z) = e^{Z(\alpha)z} \frac{H(z - \alpha)}{\Theta(z)}, \quad (8)$$

where $Z(u)$, $H(u)$, and $\Theta(u)$ are the Jacobi functions and α is an arbitrary parameter. The excitation energy Ω is related to a constant α as $\Omega = \omega_c \text{dn}(\alpha)/\kappa$. An effective potential $2 \text{sn}^2(z)$ in Eq. (7) has a period of the intersoliton distance in rescaled units $l = 2K(\kappa)$. Using translational properties of the Jacobi functions $\Theta(u + 2K) = \Theta(u)$ and $H(u + 2K) = -H(u)$ one can show that the solution (8) has the form of a Bloch wave with a quasimomentum

$$q = \frac{\pi}{2K(\kappa)} - iZ(\alpha). \quad (9)$$

The condition that propagating states have a real wave-vector q specifies the allowed values for the parameter: $\alpha = iy + K(\kappa)$ and $\alpha = iy$ with $0 < y < K' = K(\kappa')$, $\kappa' = \sqrt{1 - \kappa^2}$. The former branch is called acoustic or soliton branch, it corresponds to $0 < q < \pi/l = \pi/2K$ and has $\Omega_s(0) = 0$, $\Omega_s(\pi/l) = \omega_c \kappa'/\kappa$. The latter optic or phason branch corresponds to $q > \pi/l$ and has $\Omega > \Omega_p(\pi/l) = \omega_c/\kappa$. Thus, the spectrum of (7) exhibits a jump at the first Brillouin zone boundary remaining continuous for all other values of q . Using the series expansions [18]

$$Z(u) = \frac{2\pi}{K} \sum_{n=1}^{\infty} \frac{r^n}{1 - r^{2n}} \sin \frac{n\pi u}{K},$$

$$\text{dn}(u) = \frac{\pi}{2K} + \frac{2\pi}{K} \sum_{n=1}^{\infty} \frac{r^n}{1+r^{2n}} \cos \frac{n\pi u}{K} \quad (10)$$

with $r = \exp(-\pi K'/K)$ one can calculate spectrum in the incommensurate state for all values of anisotropy (magnetic field). At $A = A_c$ the soliton branch disappears, whereas the phason branch merges with the excitation spectrum in the commensurate state. The edge frequency of the phason branch, being a monotonically increasing function of A , exhibits a universal ratio $\Omega_p(\pi/l)|_{A=0}/\Omega_p(\pi/l)|_{A=A_c} = 2/\pi$.

A weak uniform homogeneous microwave field polarized perpendicular to the direction of an applied field \mathbf{H} generates a time-dependent force $f(t) \cos[n\varphi_0(x)]$ in the equation of motion of the phase variable $\psi(x, t)$. In the commensurate phase at $A > A_c$ when $\varphi_0(x) \equiv \pi/n$, such a force induces a conventional resonance at $\omega_c(A)$. Spatial harmonics, which can be excited by a uniform microwave field in the incommensurate state, are obtained by a Fourier decomposition of $\cos[n\varphi_0(x)] = 1 - 2\text{sn}^2(z)$. They correspond to $q = 0, 2\pi/l, \dots$. The acoustic branch has a Goldstone mode at $q = 0$ related to spontaneous breaking of translational symmetry by soliton lattice. A finite frequency resonance can occur at the wave-vector of incommensurate modulations $q^* = 2\pi/l$. The corresponding frequency $\Omega^p(q^*) = \omega_c \text{dn}(iy^*)/\kappa$ has been calculated by solving numerically equation $Z(iy^*) = i\pi/2K$. The field dependence of $\Omega^p(q^*)$ is presented in Fig.5. It is a monotonously decreasing function of field, which approaches the com-

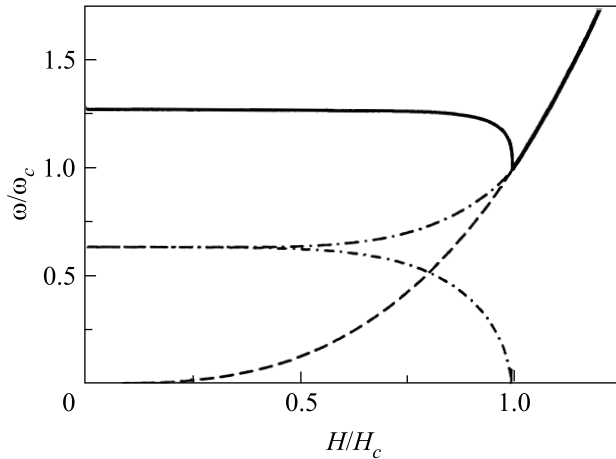


Fig.5. Field dependence of various characteristic frequencies in the incommensurate state. Anisotropy in Eq. (2) is taken $A \sim H^6$. Solid lines are frequencies excited by a uniform microwave field. Dashed line is the resonance in the commensurate phase for $b = 0$. Dot-dashed lines are the frequencies of the soliton (lower) and phason branches at the Brillouin zone boundary $q = \pi/l$

mensurate resonance frequency $\omega_c(A_c)$ at the lock-in transition with an infinite slope due to a logarithmic divergence of the intersoliton distance l . Similar to the edge frequency, a $q = 2\pi/l$ mode has a universal ratio $\Omega_p(q^*)|_{A=0}/\Omega_p(q^*)|_{A=A_c} = 4/\pi$. A flat behavior of $\Omega_p(q^*)$ as a function of h in a wide range of magnetic fields is explained by small deviations on incommensurate helix from ideal sinusoidal modulations, which transform into soliton lattice only in a narrow region near the lock-in transition. Close to H_c a coupling strength of a microwave field to the corresponding spatial harmonics becomes, however, vanishingly small: $\int_0^l \cos[6\varphi_0(x)]e^{2\pi ix/l} dx/l \simeq d/l \sim 1/\ln(H_c - H)$. This confirms conclusion of [10] about an abrupt termination of the resonance line in the commensurate state $\omega_c(H)$ at $H = H_c$. Away from H_c deep in the incommensurate state a finite frequency resonance should reappear again, although an experimental observation of this line is hindered by its weak field dependence.

Various vacancies and crystal defects, which break translational symmetry of the lattice, should destroy the $q = 0$ Goldstone mode. Here, we propose a simple model to describe oscillations of individual solitons in a field of weak pinning potential in the limit $H \rightarrow H_c$, where solitons are well separated from each other. The profile of a single soliton (3) is written as $\varphi_s(x - x_0)$, where $x_0(t)$ is a time dependent soliton position. After taking time derivative and subsequent spatial integration the kinetic energy of a soliton is found to be

$$T = \frac{4M}{n^2 d} \left(\frac{dx_0}{dt} \right)^2. \quad (11)$$

We model a weak and local pinning potential by

$$U[\varphi_s(x)] = -V a_p^2 \left(\frac{d\varphi_s}{dx} \right)^2 \Big|_{x=0}, \quad (12)$$

where $a_p \ll d$ is a characteristic spatial extension of the pinning center. In view of Eq. (5), the other possible form of the pinning energy as, e.g., $\sim \cos(n\varphi)$ is reduced to the above expression, however, it is difficult to exclude *a priori* presence of higher order gradient terms as, e.g., $(d\varphi_s/dx)^4$. Eq. (12) is easily transformed into

$$U(x_0) = \frac{4V^2 a_p^2}{n^2 d^2} \left(\tanh^2 \frac{x_0}{d} - 1 \right). \quad (13)$$

The resonance frequency of small oscillations is

$$\Omega_s = \frac{2V a_p}{\sqrt{M d^3}} = 2V a_p \left(\frac{n^6 A^3}{M^2 B^3} \right)^{1/4}. \quad (14)$$

The field dependence of the oscillation frequency is determined by field variations of the width of a domain wall

and has a faster increase with magnetic field $\Omega_s \sim H^{9/2}$ than the commensurate resonance frequency $\omega_c \sim \sqrt{A} \sim H^3$. Due to a spread of characteristic pinning energies V , which depend on microscopic structure of defects, the resonance at Ω_s should be observed as a broad line in the absorption spectrum. Note also that higher-order gradients in Eq. (12) produce a steeper increase of the oscillation frequency with magnetic field.

Finally, the microscopic row model [5, 10, 6] or the zigzag row model [3] can be used to derive the effective hydrodynamic functional 2. we modify the previous analysis by introducing an additional in-plane anisotropy induced by an orthorhombic distortion in the form $D_1 \Sigma(S_i^x)^2$. Then, the classical energy is expressed as a functional of in-plane angle φ :

$$E = \frac{\chi_{\parallel}}{2\gamma^2} (\partial_t \varphi)^2 + \frac{3}{4} J' a^2 S^2 (\partial_x \varphi)^2 - \sqrt{3} J' a S^2 \delta \partial_x \varphi + \frac{\chi_{\perp}}{24H_e^4} (H^2 \pm H_{sf}^2)^3 \cos 6\varphi, \quad (15)$$

where $\chi_{\parallel} = 2\chi_{\perp} = 1/8J$ are two principal components of the susceptibility tensor (J is the exchange constant inside chains), $\delta = J'/J_1 - 1$ is a relative change of the interchain exchange interaction, $H_e^2 = 48JJ'S^2$ is the field of a transition into the collinear phase, $\gamma = g\mu_B/2\pi\hbar$ is the gyromagnetic ratio. Parameter $H_{sf}^2 = 16JD_1S^2$ denotes a field at which the magnetic energy becomes equal to the in-plane anisotropy energy. Signs $+/-$ are chosen for $\mathbf{H} \parallel \mathbf{x}$ and $\mathbf{H} \perp \mathbf{x}$, respectively. The transition field of the commensurate-incommensurate transition in RbMnBr_3 is found from Eq. (4)

$$H_c = (\pi\delta)^{\frac{1}{3}} \sqrt{H_e^2 \pm H_{sf}^2}, \quad (16)$$

and the resonance frequency above the transition is given by the expression:

$$\left(\frac{\omega}{\gamma}\right)^2 = \frac{3}{4H_e^4} (H \pm H_{sf})^6. \quad (17)$$

The value H_{sf} (and consequently D_1) can be estimated from the splitting of the relativistic branch above the transition. Taking the difference of the resonance fields at the utmost angles of rotation at a given frequency (see inset in fig.2), one obtains $H_{sf} \simeq \sqrt{H_{\text{res}} \Delta H_{\text{res}}} \simeq 7.5 \text{ kOe}$. The value of the small in-plane anisotropy constant is estimated as $D_1 = (g\mu_B H_c)^2 / 16JS^2 \simeq 0.02 \text{ GHz}$.

4. Discussion. The results obtained in the Experiment are summarized on two frequency-field diagrams (see fig.6). Two branches of the AFMR spectrum (exchange and relativistic) have been observed in each material in the experimental frequency range. The

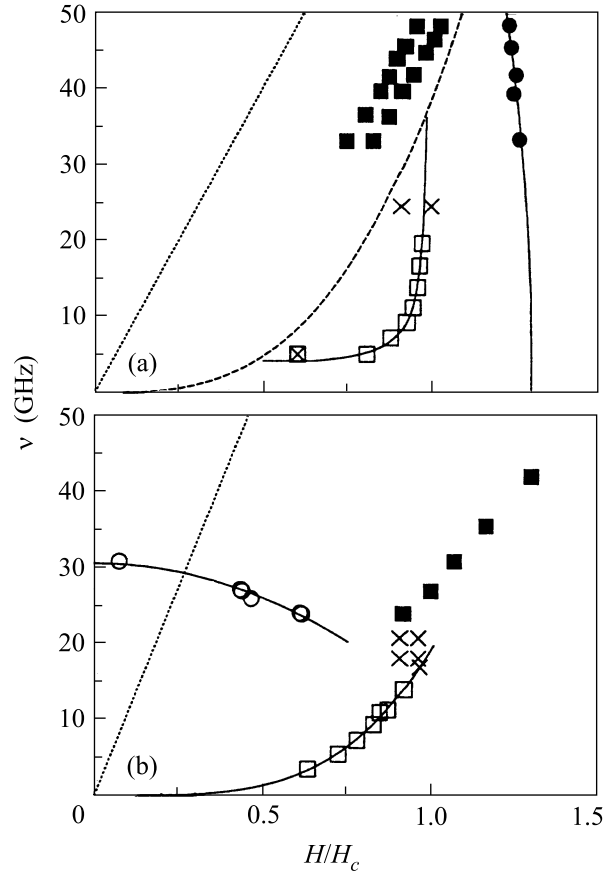


Fig.6. Frequency-field diagram $\nu(H)$ of RbMnBr_3 (a) and $\text{RbFe}(\text{MoO}_4)_2$ (b) at $T = 1.3 \text{ K}$; open and close symbols correspond to the resonance in the incommensurate and commensurate phases respectively; squares is the relativistic branch, circles is the exchange mode, \times – nonresonant singularities; \boxtimes – resonance field at $T = 2.1 \text{ K}$, solid lines – see text, dashed line is $\nu \propto H^3$ as in Fig.5, dotted line is a paramagnet with $\gamma = 2.8 \text{ GHz/kOe}$

observed optic exchange modes have different origin in the two compounds. In RbMnBr_3 such a mode appears due to a noncollinear spin structure and softens at the transition into the collinear phase $H = H_e \simeq 39 \text{ kOe}$ [9], while in $\text{RbFe}(\text{MoO}_4)_2$ an optic branch corresponds to uniform out-of-phase oscillations of weakly interacting neighboring spin planes [11]. Corresponding field dependencies are shown in fig.6 by solid lines. Further, we shall discuss only the behavior of the relativistic branch.

First of all, one should note, that the field dependencies of the relativistic branches found in both structures are quite similar: steep increase of the gap in the incommensurate phase in the vicinity of the transition field followed by a jump to a commensurate resonance frequency. As the observed resonance mode at $H > H_c$ both in RbMnBr_3 and in $\text{RbFe}(\text{MoO}_4)_2$ is associated

with the uniform oscillations of the spin system in the easy plane, one can also suggest this branch at $H < H_c$ to have the same nature in both compounds.

We can, however, exclude, this interpretation on the basis of our theoretical calculations of the long-wave oscillation spectrum in the weakly modulated triangular spin system with the strong easy-plane anisotropy (see fig.5). The energy of the “phason” branch at the wave vector $q = 2\pi/l$ excited by a uniform SHF-field decreases in magnetic field and is, in addition, practically dispersionless except for a small region near H_c . Similar mode has been recently observed in the collinear antiferromagnet CuB_2O_4 in one of the low-field phases, which has a long-wave modulation of the spin structure [19]. At the same time, oscillations at $q = 0$ remain gapless because they correspond to uniform shifts of the whole soliton lattice at no energy cost.

We suggest a different interpretation of the observed resonance mode in the incommensurate states of both compounds. The field increasing gap of the magnetic resonance may be attributed to a local domain walls at various defects of the crystal lattice (vacancies, dislocations etc.). Local oscillations of domain walls have a characteristic frequency $\nu(H) \sim H^{9/2}$ instead of a less steep dependence $\sim H^3$ usual for triangular antiferromagnets in weak magnetic fields. This is in qualitative agreement with the experimental result obtained for $\text{RbFe}(\text{MoO}_4)_2$: the guide-to-eye line in fig.6b fits the data by formula $\nu \sim (H/H_c)^4$, which agrees well with the exponent $n = 9/2$ suggested from the theoretical study. We find, however, a strong discrepancy with the experimental behavior of the resonance mode in RbMnBr_3 . First, the observed field dependence is much steeper $\sim H^n$ with $n = 10-12$ and second, it has a gap at $H = 0$ due to the hyper-fine interaction in Mn^{2+} ions. Besides, we have observed a strong temperature evolution of the resonance line in the temperature range 1.3–2.2 K (well below $T_N = 8.5$ K). On heating, the absorption maximum shifts to lower fields (see. fig.3), which is unusual for a field-increasing branches in the presence of a hyper-fine gap reduced by temperature. Thus, the origin of the field and temperature dependent gap of the acoustic resonance branch in RbMnBr_3 requires further discussion.

The authors are grateful to V. Glazkov, V. Marchenko, A. Smirnov and L. Svistov for useful discussions. The work of L.A.P. and S.S.S. was partially supported by RFBR, grant # 04-02-17294. S.S.S also thanks the National Science Support Foundation for the financial help.

-
1. I. E. Dzyaloshinskii, ZhETF **46**, 1420 (1964) [Sov. Phys. JETP **19**, 960 (1964)].
 2. D. Visser, G. C. Verschoor, and D. J. W. Ijdo, Acta Crystallogr. **B36**, 28 (1980).
 3. T. Kato, J. Phys. Soc. Jpn. **71**, 300 (2002).
 4. L. Heller, M. F. Collins, Y. S. Yang, and B. Collier, Phys. Rev. **B49**, 1104 (1994).
 5. W. Zhang, W. M. Saslow, and M. Gabay, Phys. Rev. **B44**, 5129 (1991); W. Zhang, W. M. Saslow, M. Gabay, and M. Benakli, Phys. Rev. **B48**, 10204 (1993).
 6. M. E. Zhitomirsky, Phys. Rev. **B54**, 353 (1996).
 7. S. A. Klimin, M. N. Popova, B. N. Mavrin et al., Phys. Rev. **B68**, 1744XX (2003).
 8. G. Gasparovic, M. Kenzelmann, C. Broholm et al., unpublished.
 9. I. M. Vitebskii, O. A. Petrenko, S. V. Petrov, and L. A. Prozorova, Sov. Phys. JETP **76**, 178 (1993).
 10. M. E. Zhitomirsky, O. A. Petrenko, and L. A. Prozorova, Phys. Rev. **B52**, 3511 (1995).
 11. L. E. Svistov, A. I. Smirnov, L. A. Prozorova et al., Phys. Rev. **B67**, 094434 (2003).
 12. I. A. Zaliznyak, N. N. Zorin, and S. V. Petrov, JETP Lett. **64**, 473 (1996).
 13. L. A. Prozorova, S. S. Sosin, D. V. Efremov, S. V. Petrov, Sov. Phys. JETP **85**, 1035 (1997).
 14. I. E. Dzyaloshinskii, ZhETF **47**, 992 (1964) [Sov. Phys. JETP **20**, 665 (1965)].
 15. P. Lebowitz and M. J. Stephen, Phys. Rev. **163**, 376 (1967); A. L. Fetter and M. J. Stephen, Phys. Rev. **168**, 475 (1968).
 16. W. L. McMillan, Phys. Rev. **B16**, 4655 (1977).
 17. V. L. Pokrovsky and A. L. Talapov, Sov. Phys. JETP **48**, 579 (1978).
 18. E. T. Whittaker and G. N. Watson, *A Course of Modern Analysis*, Cambridge Press, London, 1963.
 19. A. I. Pankrats, G. A. Petrakovskij, M. A. Popov et al., Pis'ma ZhETF **78**, 1058 (2003).